Eur. Phys. J. A **3**, 133–138 (1998)

THE EUROPEAN PHYSICAL JOURNAL A
© Springer-Verlag 1998

Recoil distance half-life measurements of the excited states in ^{145}Sm

A.M. El-Badry[1,a], T. Kuroyanagi[1], S. Mitarai[1], A. Odahara[1,b], Y. Gono[1], S. Morinobu[1], K. Ogawa[2]

[1] Department of Physics,Kyushu University, Hakozaki 6-10-1, Higashi-ku, Fukuoka 812-8581, Japan
[2] Department of physics, Chiba University, Chiba 263, Japan

Received: 9 September 1997 / Revised version: 12 June 1998
Communicated by K. Nakai

Abstract. A recoil distance method was used to measure half-lives of the excited states of ^{145}Sm. The reaction used was ^{139}La(^{10}B, 4n)^{145}Sm. A plunger system was used. Half-lives were determined for two excited states for the first time. The yrast $27/2^+$ state was found to have a half-life of 1.1 ± 0.2 ns corresponding to the retardation of 3.1×10^{-4} comparing with the single particle estimate of M1. The excitation energy of this state was well reproduced by the shell model calculation having a mixed configuration of $[\pi\{h_{11/2}(g_{7/2})^{-2}\ (d_{5/2})^{-1}\ \}_{10}\text{-},\ \nu f_{7/2}] + [\pi\{h_{11/2}(g_{7/2})^{-1}\}_{9}\text{-},\nu h_{9/2}]$. Another retarded E1 transition was also found in a decay of a $21/2^+$ state. Its retardation was 1.6×10^{-4} comparing with the single particle value.

PACS. 21.10.-k Properties of nuclei; nuclear energy levels – 27.60.+j $90 \leq A \leq 149$

1 Introduction

In the isotones with N=82, ^{146}Gd [1], ^{148}Dy [2] and ^{150}Er [3], the 10^+ states of a $(\pi h_{11/2})^2$ configuration are known to exist systematically. These states in ^{148}Dy and ^{150}Er are isomers with relatively long half-lives of 0.471 μs and 2.55 μs, respectively. The yrast states of a spin 27/2 are known to be isomers of negative parity in neighboring isotones with N=83, ^{147}Gd [4], ^{149}Dy [5] and ^{151}Er [6] . They were interpreted to have a configuration of $[(\pi h_{11/2})^2 \otimes \nu f_{7/2}]$. However a state with the same configuration has not been identified in N=82 and 83 isotones with Z<64 [7]. A 27/2 yrast state in ^{145}Sm was reported to have positive parity [7]. The origin of this parity change of the 27/2 yrast states in N=83 isotones at Z=64 subshell-closure has not been understood. It is essential to measure a half-life of the $27/2^+$ yrast state in ^{145}Sm and to assign its configuration to solve the problem mentioned above.

High-spin states of ^{145}Sm were reported [7,8] previously. They were studied by in-beam gamma and electron spectroscopic techniques and were interpreted within the framework of the empirical shell model (ESM) [8] and the deformed independent particle model (DIPM) [7]. Many low-spin states of ^{145}Sm were also known [9] from studies of a β-decay of ^{145}Eu and the ^{144}Nd(α,3n),^{144}Sm(d,p) reactions.

In this report, the results of a half-life measurement of the low-lying states in ^{145}Sm are presented.

2 Experimental procedures

The nucleus ^{145}Sm was produced by the ^{139}La(^{10}B, 4n)^{145}Sm reaction. The half-lives of excited states of ^{145}Sm were measured by a recoil distance method (RDM). The ^{10}B beam was provided by the Kyushu University tandem accelerator. The excitation function was taken in the energy range of the ^{10}B beam from 42 to 52 MeV. The optimum energy for the 4n emission channel was determined to be 49 MeV which agreed with a result calculated by using a computer code CASCADE [10].

A La target of a 0.22 mg/cm^2 thickness was prepared by evaporation on a 2 mg/cm^2 Au foil. It was crucial to keep the surface of the target extremely flat for this experimental method. A target holder was made to realize a flat surface by giving uniform tension to the target foil. A conventional plunger system was used for RDM. A stopper for the recoil nuclei and the beam was made of a Pb foil of an 86 mg/cm^2 thickness. The target was made to move in a continuous range from 10 μm to 10 mm with respect to the fixed stopper. Since the velocity of recoil nuclei was calculated to be 1.76 mm/ns as explained below, the corresponding time range was from 5.7 ps to 5.7 ns. A fixed distance of 58 mm was also used when it was necessary. This distance corresponds to 33 ns of flight time.

Singles γ-ray spectra were taken by using a HPGe (GMX) detector of 20 % relative efficiency. The detector

[a] Present address: Department of Physics, El-Minia University, El-Minia, Egypt
[b] Present address: Department of Engineering, Nishinippon Institute of Technology, Kanda, Fukuoka 800-03, Japan

was placed 64 mm apart from the stopper foil and at 0 ^{0} with respect to the beam axis. A low energy photon spectrometer (LEPS) with a high energy resolution was also used to separate Doppler-shifted and unshifted peaks of low energy γ-rays. LEPS was placed at the same position as GMX. An absorber which consisted of a 4 mm Cu and a 1 mm Al plate was set in front of the γ-ray detectors to suppress X-rays. The γ-ray spectra were taken at 20 positions of different target-stopper distances. These data taken by GMX and LEPS at each position were collected for the integrated beam charges of 100 μC and 400 μC, respectively.

Singles γ-ray spectrum was also taken at 125 ^{0} with respect to the beam axis to obtain γ-ray relative intensities. In this case a La target of 1 mg/cm^2 was used. The background spectra originating from reactions of ^{10}B bombardments on targets of Au, Pb, ^{16}O, ^{27}Al at the same beam energy of 49 MeV were also measured. The background from these reactions were unavoidable in the present experimental setup. These measurements worked effectively to subtract the background components from the γ-ray peaks of ^{145}Sm. The γ-ray energy and efficiency calibrations of Ge detectors were made by using a standard source of ^{152}Eu.

3 Analyses and results

3.1 Spectrum analysis

Thirty three γ-rays of ^{145}Sm were identified comparing the γ-ray energies and intensities obtained in this experiment with those reported previously [7, 8]. Their energies and intensities are listed in Table 1. The relative intensities were different from those given in [7]. The origin of differences was attributed to a difference of target thicknesses, namely 51 and 1 mg/cm^2 in cases of [7] and the present experiment, respectively. In the former case, the ^{10}B beam was stopped in the target and the energy-degraded beam produced more excited states at lower excitation energies. It turned out that the present reaction populated up to the (31/2) state at 5029 keV. Twelve γ-rays deexciting the states up to the $27/2^+$ state at 3922 keV appeared with reasonable intensities to give information on half-lives.

High energy parts of γ-ray spectra taken by GMX at various target-stopper distances are shown in Fig. 1. The γ-ray peaks of 944.8, 1104.7 and 1331.4 keV transitions were seen to be shifted to 950.5, 1111.5 and 1338.8 keV. These energy differences were used to extract the recoil velocity v of ^{145}Sm. The deduced velocity was 1.76±0.02 mm/ns (v/c=0.00585±0.00007). This value is consistent with that calculated taking into account the energy losses of both the projectile and the recoiling nucleus ^{145}Sm in the target. It is clear from the intensity ratios of the shifted and unshifted peaks in Fig. 1 that the 1105 keV γ-ray deexcites a state with a relatively long half-life while 945 and 1331 keV γ-rays deexcite those with short half-lives. Low energy parts of γ-ray spectra taken by LEPS are shown in Fig. 2. It is clear that the use of LEPS with a high energy resolution was inevitable because the energy differences of the shifted and unshifted peaks are small as seen in the figure.

To analyze areas of both the sifted and unshifted peaks, a computer code GF2 was used. This program fits peaks by using three components, i.e. a Gaussian peak of main component, a skewed Gaussian of a low energy tail and a step function of the background. An example of peak fits is shown in Fig. 3. The broadening of the sifted peak width is consistent with the calculated energy broadening of recoiling nuclei ^{145}Sm in the target. Corrections such as a dead time of the data taking system and γ-ray detection efficiencies including solid angles were taken into account. Since the target was moved with respect to the stopper which was placed at a fixed position, it was necessary in the analyses of the peak areas to make corrections for the solid angles subtended by the Ge detectors. The dependence of the solid angle correction on half-lives was also taken into account. They were necessary when the target-

Table 1. Relative intensities of γ-rays of ^{145}Sm

E_γ(keV)	I_γ	E_i(keV)	I_i	→	I_f [a]
140.2	23.9(5)	3120	$23/2^+$	→	$21/2^+$
161.2 [b]	7.0(4)	5030	(31/2)	→	(29/2)
		3484	$25/2^+$	→	(21/2)
180.5	46.9(9)	2231	$17/2^-$	→	$15/2^-$
189.1	26.5(8)	3120	$23/2^+$	→	$21/2^+$
191.8	5.6(2)	4421	$29/2^+$	→	$27/2^+$
210.0	4.3(2)	3140			
219.8	12.0(6)	2930	$21/2^+$	→	$19/2^-$
236.6	0.7(1)	3376			
268.6	26.1(3)	2980	$21/2^+$	→	$19/2^-$
281.9	1.6(2)	4869			
289.1	1.9(1)	5030	(31/2)	→	(29/2)
306.3	4.8(4)	4229	(27/2)	→	$27/2^+$
364.1	36.5(4)	3484	$25/2^+$	→	$23/2^+$
391.6	4.3(2)	3322	(21/2)	→	$21/2^+$
394.7	2.6(5)	4315			
396.8	6.0(2)	3376			
438.2	21.8(4)	3922	$27/2^+$	→	$25/2^+$
480.5	36.9(4)	2711	$21/2^-$	→	$17/2^-$
493.7	32.6(33)	2930	$21/2^+$	→	$17/2^+$
499.0	7.3(3)	4421	$29/2^+$	→	$27/2^+$
639.9	1.1(3)	5030	(31/2)	→	(29/2)
714.6	2.6(5)	5030	(31/2)	→	$29/2^+$
734.8	9.9(4)	2965	$19/2^+$	→	$17/2^-$
744.6	5.9(3)	4229	(27/2)	→	(21/2)
944.8	52.7(5)	2050	$15/2^-$	→	$13/2^+$
1066.7	3.7(3)	4389	(27/2)	→	(21/2)
1104.7	100.0(9)	1105	$13/2^+$	→	$7/2^-$
1257.2	10.2(4)	4741	(29/2)	→	$25/2^+$
1270.1	2.7(3)	4389	(27/2)	→	$23/2^+$
1331.4	37.6(7)	2436	$17/2^+$	→	$13/2^+$
1385.0	4.5(4)	4869	(29/2)	→	$25/2^+$
1467.8	1.5(3)	4587			
1537.8	4.5(4)	1538	$11/2^-$	→	$7/2^-$

a. Spins and parities are taken from [7]
b. Unresolved doublet

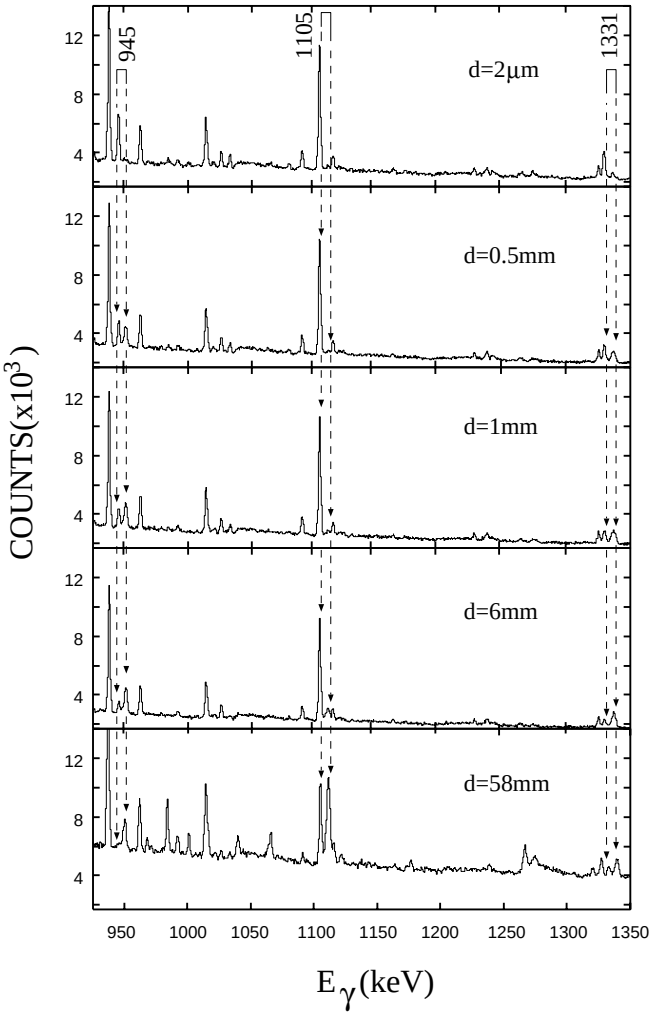

Fig. 1. High energy parts of the γ-ray spectra taken by GMX at various target-stopper distances

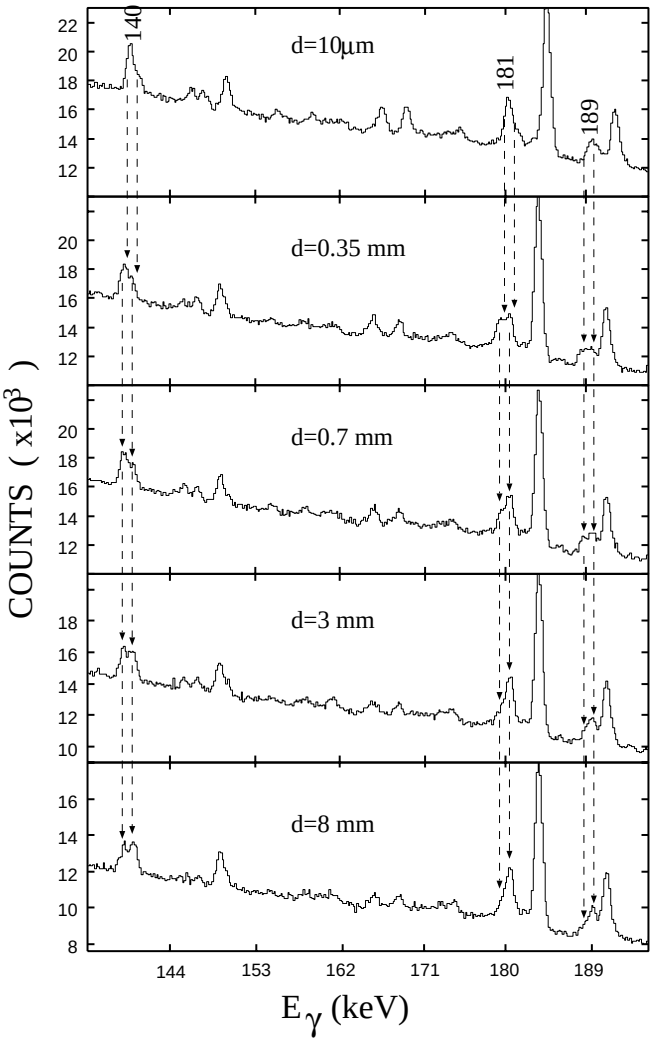

Fig. 2. Low energy parts of the γ-ray spectra taken by LEPS at various target-stopper distances

stopper distance was large and the decay curves of γ-rays contained relatively long lived components.

In addition to these corrections, γ-rays originated from the unwanted reaction products caused sever problems in some cases. The 269 keV γ-ray peak of ^{145}Sm overlapped with a γ-ray of the same energy emitted from the Coulomb excitation of ^{197}Au. This kind of accidental overlaps also occurred for other peaks of 140, 364 and 438 keV. In order to subtract the background components the γ-ray spectra from the reactions of the 49 MeV ^{10}B beam with targets of Au, Pb, O and Al were also measured. The contributions of these contaminant components were estimated by using the intensities of the isolated peaks stemmed from the same origin with a help of the known intensity ratios.

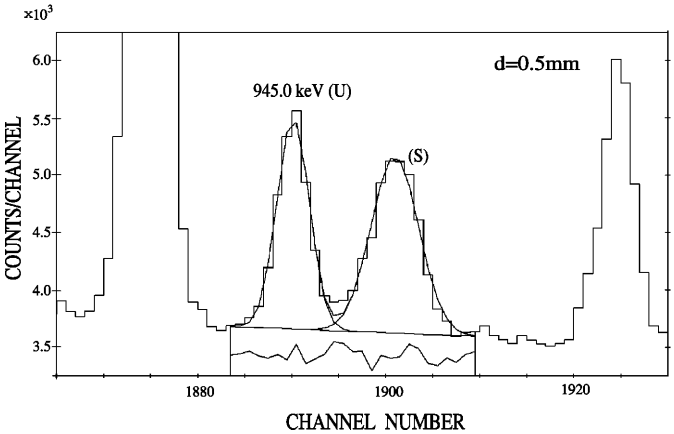

Fig. 3. An example of peak fits for a shifted and unshifted 945 keV γ-ray made by using GF2

3.2 Decay curve

In RDM, the distances between a target and a stopper correspond to flight times of recoiling nuclei. Therefore decay curves of γ-rays of interest were made by plotting the ratios between areas of unshifted peaks and sums of unshifted and shifted peaks as a function of the distance. The analyses were also made by using the yields either of the Pb KX-rays or of γ-rays from the Coulomb excitation

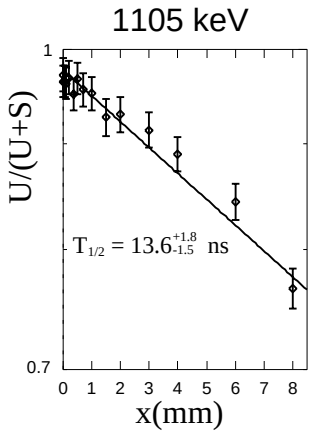

Fig. 4. A decay curve of the 1105 keV transition in ^{145}Sm

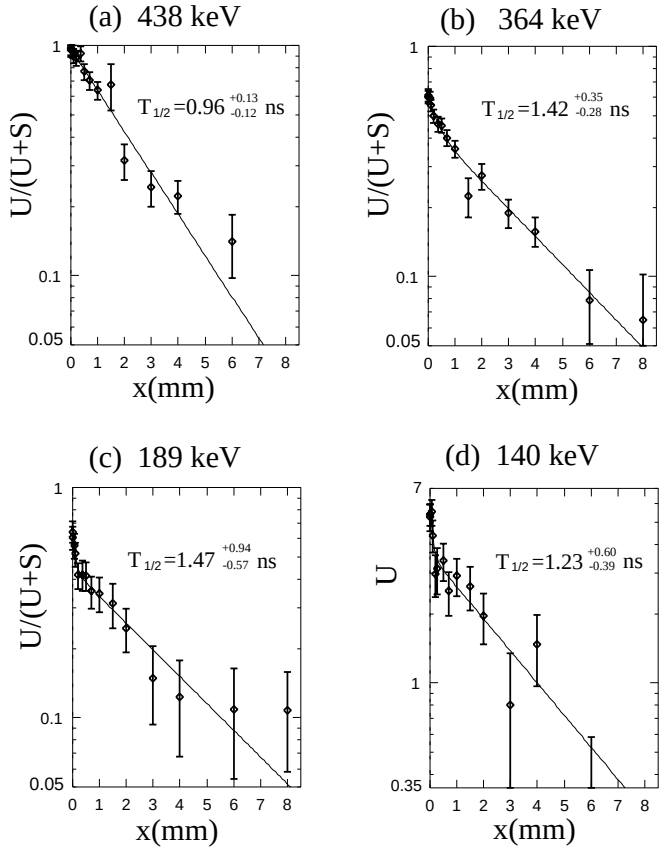

Fig. 5. Decay curves of (a) 438-, (b) 364-, (c) 189- and (d) 140-keV transitions. In case of the 140 keV transition the intensities of only unshifted peaks are plotted because of the contamination of the shifted peaks. Half-lives given in the spectra are components extracted from each spectrum and considered to be the same

of Au for normalization. Examples of the decay curves are shown in Figs.4-6. Half-lives of the excited states of ^{145}Sm were extracted by least square fittings of these curves to the multi-component decay curves of,

$$I_u/(I_u + I_s) = \Sigma N_i \exp(-\lambda_i d/v)$$

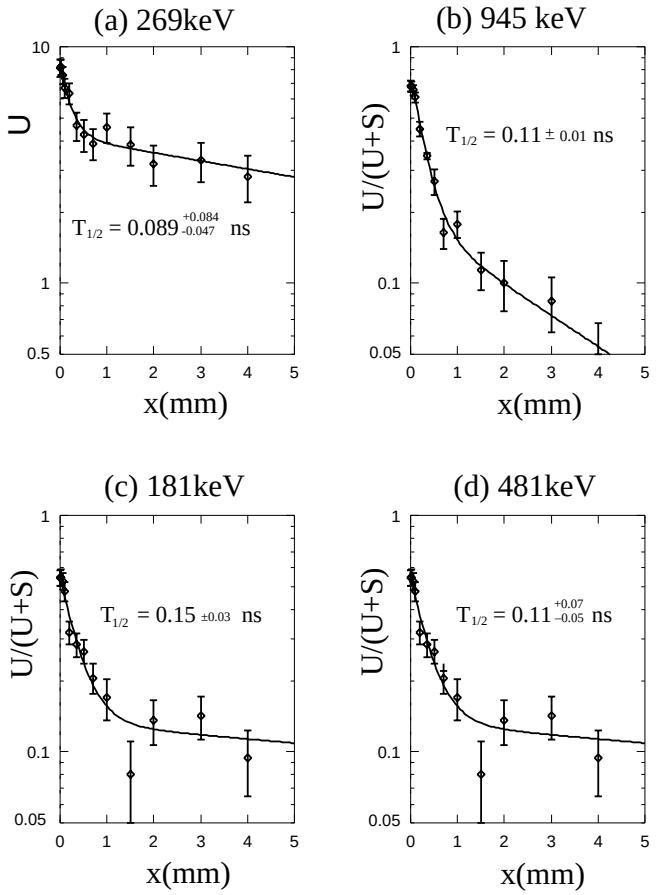

Fig. 6. Decay curves of (a) 269-, (b) 945-, (c) 181- and (d) 481-keV transitions. The shifted peaks of the 269 keV transition had the same problem as in the case of 140 keV transition in Fig. 4. Half-lives given in the figures are the same as in Fig. 5

where I_s and I_u are intensities of shifted and unshifted peaks, d and v are the target-stopper distance and the recoil velocity of the reaction products, respectively. N_i and λ_i are fitting parameters. Two independent analyses were made by using different normalizations mentioned above. Those results agreed with each other for all the analyzed γ-rays within the experimental accuracies.

A half-life deduced from the decay curve of Fig. 4 for the 1105 keV γ-ray deexciting the $13/2^+$ state was (13.6 $\pm$ 0.7) ns which agrees well with that reported previously [11]. A half-life of $(0.96^{+0.13}_{-0.12})$ ns was obtained from the decay curve of the 438 keV γ-ray which is shown in Fig. 5(a). The same half-lives within the experimental accuracies of $(1.42^{+0.35}_{-0.28})$, $(1.47^{+0.94}_{-0.57})$ and $(1.23^{+0.60}_{-0.39})$ ns were found in the decay curves of 364, 189 and 140 keV γ-rays as shown in Fig. 5(b), (c) and (d). These γ-rays deexcite the states populated more than 64% through the 438 keV γ-ray. The weighted average of these half-lives was (1.1$\pm$0.2) ns. This half-life was attributed to that of the $27/2^+$ state at 3922 keV because the decay curve of 438 keV γ-ray showed only one component though this state was populated at least by three relatively weak γ-rays.

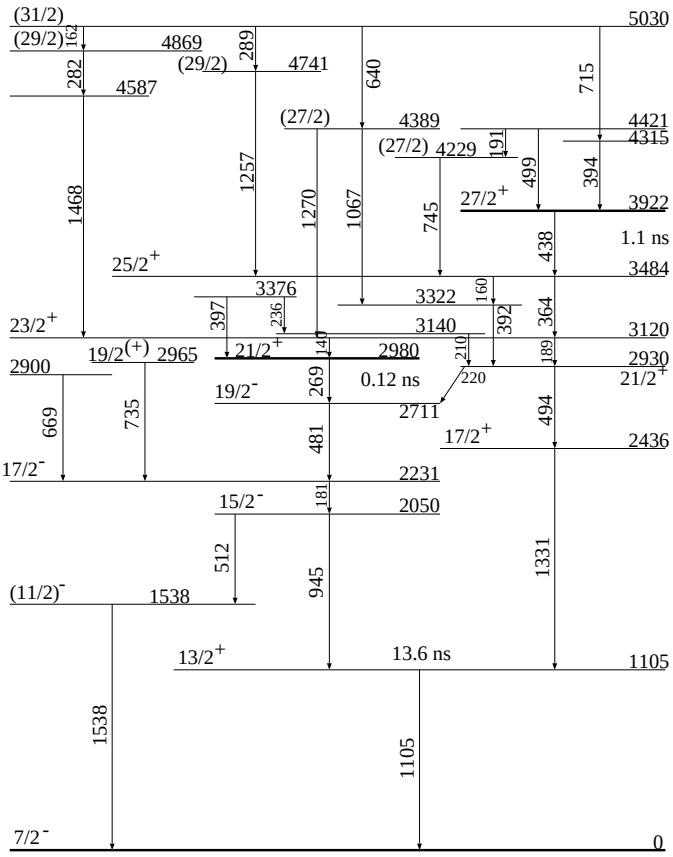

Fig. 7. Partial level scheme of ^{145}Sm. Half-lives determined in the present work are also shown

Table 2. Summary of half-life analyses

E_γ	half-lives (ns)		
(keV)	I	II	III
140	$0.04\ ^{+0.07}_{-0.03}$	$1.2\ ^{+0.6}_{-0.4}$	
	(0.36)	(0.64)	
181	0.15 ± 0.03	$9.77\ ^{+\infty}_{-5.8}$	
	(0.76)	(0.24)	
189	$0.04\ ^{+0.08}_{-0.02}$	$1.5\ ^{+0.9}_{-0.6}$	
	(0.32)	(0.68)	
220	$0.19\ ^{+0.28}_{-0.12}$	$1.9\ ^{+107}_{-1.4}$	
	(0.66)	(0.34)	
269	$0.09\ ^{+0.08}_{-0.05}$	$5.0\ ^{+10}_{-2.5}$	
	(0.50)	(0.50)	
364	$0.14\ ^{+0.16}_{-0.08}$	$1.4\ ^{+0.4}_{-0.3}$	
	(0.34)	(0.66)	
438	$0.96\ ^{+0.13}_{-0.12}$		
	(1)		
481	$0.11\ ^{+0.07}_{-0.05}$	$5.5\ ^{+3.5}_{-1.7}$	
	(0.47)	(0.53)	
494	$0.02\ ^{+0.93}_{-0.02}$	$0.19\ ^{+0.08}_{-0.06}$	$17\ ^{+\infty}_{-10}$
	(0.08)	(0.67)	(0.25)
945	$0.014\ ^{+0.033}_{-0.011}$	0.11 ± 0.01	1.3 ± 0.5
	(0.12)	(0.68)	(0.20)
1105	13.6 ± 0.7		
	(1)		
1331	$0.02\ ^{+0.15}_{-0.02}$	0.17 ± 0.04	$7.1\ ^{+\infty}_{-4.3}$
	(0.12)	(0.73)	(0.15)

Notes: Decay curves were analyzed including 1,2 and 3 components.
I,II,III stand for each component put in order of a half-life.
Numbers in parentheses are those of relative intensity

The decay curve of the 269 keV γ-ray has a component of $(0.089^{+0.084}_{-0.047})$ ns as can be seen in Fig. 6(a). This component was interpreted to be the same within the experimental accuracy as those of (0.11 ± 0.01), (0.15 ± 0.03) and $(0.11^{+0.07}_{-0.05})$ ns appeared in the decay curves of cascade γ-rays of 945, 181 and 481 keV, respectively, as seen in Figs.6(b),(c),(d). The weighted average of these values was (0.12 ± 0.02) ns which was taken as a half-life of the $21/2^+$ state at 2980 keV. Among them three γ-rays of 269, 481 and 181 keV had components of about 5ns as seen in Table 2. This component should be attributed to some side-feeding. But it could not be assigned to any level in this work. These results are given in the level scheme of Fig. 7 and listed in Table 2.

Components of $(0.19^{+0.08}_{-0.06})$ and (0.17 ± 0.04) ns were found in the decay curves of the 494 and 1331 keV cascade γ-rays, respectively. However a 1.1 ns component could not be extracted though the states deexcited by these γ-rays should be populated through the $27/2^+$ state at 3922 keV. Therefore this half-life could not be assigned to a specific state in this work.

4 Discussion

The yrast $27/2^+$ state in ^{145}Sm was established at 3922 keV in [7]. The half-life of this state was determined to be 1.1 ns in the present work. The multipolarity of the 438 keV γ-ray was known to be M1 from both the conversion coefficient [8] and the angular distribution coefficients [7, 8]. These experimental facts indicate that this M1 transition is retarded by a factor of 3.1×10^{-4} compared with a single particle estimate. However the excitation energy of this state could not be reproduced by ESM and DIPM. The shell model calculation made by taking into account the interactions between different configurations could reproduce fairly well this state as explained below.

Based on the Z=64 subshell closure, properties of low-lying states in ^{145}Sm may be discussed in terms of a small number of active protons coupled with a neutron. For the low-lying negative parity states including the $7/2^-$ ground state, a configuration $[\pi(1g_{7/2},2d_{5/2})^{-2} \otimes \nu(2f_{7/2},1h_{9/2})^1]$ was adopted in the present calculation and the configuration $[\pi(1g_{7/2},2d_{5/2})^{-3}(1h_{11/2})^1 \otimes \nu(2f_{7/2},1h_{9/2})^1]$ for the excited positive parity states such as the $25/2^+$ and $27/2^+$ states.

The single-particle energies and two-body effective interactions for protons were selected to reproduce the low-lying energy levels in the N=82 isotones. In the present calculation the surface delta interaction with $V_{T=1}$=0.35 MeV was adopted. Neutron states were known from the spectrum of ^{147}Gd [12] and the energy spacing of

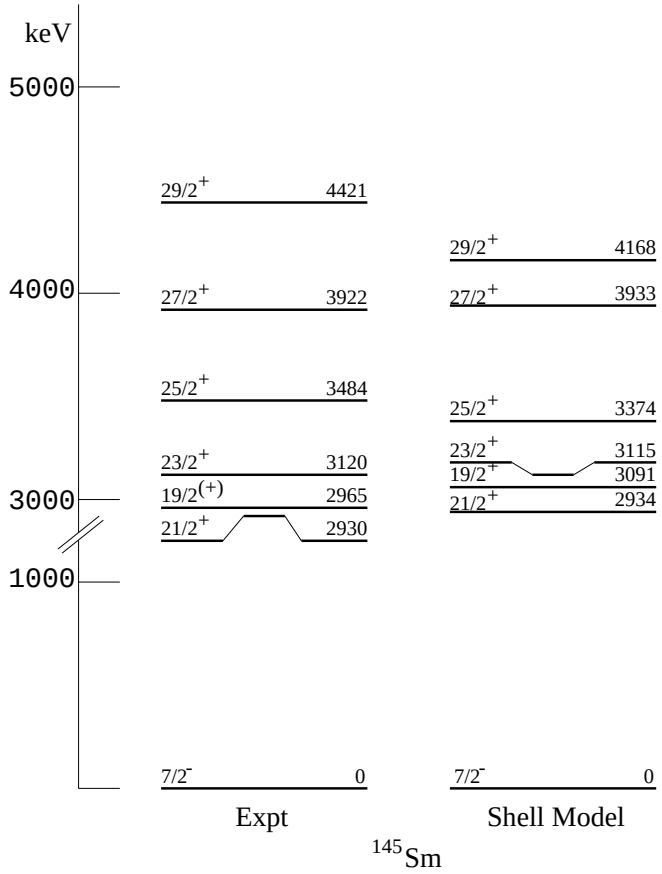

Fig. 8. The excited states in ^{145}Sm resulted in the experiments are compared with those of the shell model calculation

$\varepsilon(1h_{9/2})_n - \varepsilon(2f_{7/2})_n = 1.48$ MeV was used in the calculation. For the effective proton-neutron interactions we adopted the Yukawa type interaction with Serber mixture (V_{SE}=V_{TO}= −40 MeV) to reproduce the low-lying spectrum of ^{146}Eu [13].

The calculated energy spectrum of ^{145}Sm is shown in Fig. 8. As the figure shows, the $27/2^+$ state was reproduced at 3.93 MeV which was 0.56 MeV higher than the $25/2^+$ state.

The resulted wave function of the $27/2^+$ state showed that its main components were [^{144}Sm (J^π=10^- at 4.70 MeV) ⊗ $\nu(f_{7/2})$: J^π=$27/2^+$] and [^{144}Sm (J^π=9^- at 3.46 MeV) ⊗ $\nu(h_{9/2})$: J^π=$27/2^+$]. If one adopts a weak coupling between the ^{144}Sm core [12] and a single neutron, these two states are predicted at about 4.7 and 4.9 MeV, respectively, in ^{145}Sm. However actually the interaction between these two $27/2^+$ states were strong due to the proton-neutron interaction and the lowest eigen state was obtained at 3.93 MeV. Thus the $h_{9/2}$ neutron state plays an important role to reproduce the $27/2^+$ state. On the other hand the $25/2^+$ state predicted at 3.37 MeV was mainly composed of [^{144}Sm (J^π=9^- at 3.46 MeV) ⊗ $\nu(f_{7/2})$: J^π=$25/2^+$]. For this state the $h_{9/2}$ neutron state did not affect the excitation energy, because the [^{144}Sm (J^π=8^- at 3.38 MeV) ⊗ $\nu(h_{9/2})$: J^π=$25/2^+$] component was predicted at about 1.4 MeV higher than the $25/2^+$ state with the $f_{7/2}$ neutron and the coupling between these two states were very weak. Thus we conclude the coupling between the $\nu(f_{7/2})$ and $\nu(h_{9/2})$ states is essential for the existence of the $27/2^+$ isomer in ^{145}Sm.

Since the configuration of the $25/2^+$ state was known to be [$\pi\{h_{11/2}(g_{7/2})^{-1}\}_{9^-}$,$\nu f_{7/2}$] [8] and the two main components of the $27/2^+$ state are obtained to be [^{144}Sm (J^π=10^-: seniority=4) ⊗ $\nu(f_{7/2})$: J^π=$27/2^+$] and [^{144}Sm (J^π=9^- :seniority=2) ⊗ $\nu(h_{9/2})$: J^π=$27/2^+$], an M1 transition is forbidden between these $27/2^+$ and $25/2^+$ states in the first order approximation. This is consistent with the fact that the $27/2^+$ state is an isomer as established in the present work.

A half-life of 0.12 ns was also observed in the present work and attributed to that of the $21/2^+$ state at 2980 keV in ^{145}Sm. This state decays by an E1 transition of 269 keV [8]. Comparing with an E1 single particle estimate, this transition is retarded by a factor of 1.6×10^{-4}. This positive parity state was suggested to have octupole collectivity [8]. However a collective E1 operator is proportional to a product of collective parameters β_2 and β_3, and a large component of octupole phonon should induce fast E1 transition. Therefore present result indicates that there is not a large admixture of an octupole component in this $21/2^+$ state.

One of the authors (A.M.E) thanks to the Channel System of Egyptian Ministry of Higher Education for giving a chance to work on this subject at Kyushu University. She also thanks to the members of Kyushu University tandem accelerator laboratory for warm hospitality given to her during her stay. We are very much indebted to Dr.D.C. Radford for him to have provided the data analysis program GF2 without which data analyses could not be proceeded.

References

1. L. K. Peker, Nucl. Data Sheets **60**, 953 (1990)
2. L. K. Peker, Nucl. Data Sheets **59**, 393 (1990)
3. Y. H. Chung et al., Phys. Rev. **C29**, 2153 (1984)
4. E. der Mateosian, L. Peker, Nucl. Data Sheets **66**, 705 (1992)
5. J. A. Szucs, M. W. Johns and B. Singh, Nucl. Data Sheets **46**, 1 (1985)
6. S. Andre et al. , Z. Phys. **A337**, 349 (1990)
7. A. Odahara et al., Z. Phys. **A350**, 185 (1994), Nucl. Phys. A620, 363 (1997)
8. M. Piiparinen et al., Z. Phys. **A338**, 417 (1991)
9. L. K. Peker, Nuclear Data Sheets **49**, 1 (1986)
10. F. Pülhofer, Nucl. Phys. **A280**, 267 (1977)
11. Z. Haratym et al., Nucl. Phys. **A276**, 299 (1977)
12. Table of Isotopes 8th edition, ed. R. B. Firestone and V. S. Shirley (1996) John Wiley and Sons Inc
13. E. Ott et al., Z. Phys. **A348**, 57 (1994)